Real-time detection of PRT1-mediated ubiquitination via fluorescently labeled substrate probes

Augustin C. Mot,[1,2] Erik Prell,[3] Maria Klecker,[1,2] Christin Naumann,[1,2] Frederik Faden,[1,2] Bernhard Westermann[3] & Nico Dissmeyer[1,2,*]

[1] Independent Junior Research Group on Protein Recognition and Degradation, Leibniz Institute of Plant Biochemistry (IPB), Weinberg 3, D-06120 Halle (Saale), Germany

[2] ScienceCampus Halle – Plant-based Bioeconomy, Betty-Heimann-Str. 3, D-06120 Halle (Saale), Germany

[3] Department of Bioorganic Chemistry, Leibniz Institute of Plant Biochemistry (IPB), Weinberg 3, D-06120 Halle (Saale), Germany

[*] Correspondence should be addressed to N.D. (phone: +49 176 2355 8710; nico.dissmeyer@ipb-halle.de, Twitter: @NDissmeyer).

RUNNING TITLE

Live assays with fluorescent N-end rule substrates

Total word count

main body (Introduction: 1639, Materials and Methods: 2081, Results: 1174 , Discussion: 2053, Acknowledgements: 204)

Number of figures/tables/supporting information

3 figures (all color), no tables, 1 Supporting Figure, 2 Supporting Tables, 1 Supporting Methods

SUMMARY

- **The N-end rule pathway has emerged as a major system for regulating protein functions by controlling their turn-over in medical, animal and plant sciences as well as agriculture. Although novel functions and enzymes of the pathway were discovered, ubiquitination mechanism and substrate specificity of N-end rule pathway E3 Ubiquitin ligases remained elusive. Taking the first discovered *bona fide* plant N-end rule E3 ligase PROTEOLYSIS1 (PRT1) as a model, we use a novel tool to molecularly characterize polyubiquitination live, in real-time.**
- **We gained mechanistic insights in PRT1 substrate preference and activation by monitoring live ubiquitination by using a fluorescent chemical probe coupled to artificial substrate reporters. Ubiquitination was measured by rapid in-gel fluorescence scanning as well as in real time by fluorescence polarization.**
- **Enzymatic activity, substrate specificity, mechanisms and reaction optimization of PRT1-mediated ubiquitination were investigated *ad hoc* in short time and with significantly reduced reagent consumption.**
- **We demonstrated for the first time that PRT1 is indeed an E3 ligase, which was hypothesized for over two decades. These results demonstrate that PRT1 has the potential to be involved in polyubiquitination of various substrates and therefore pave the way to understanding recently discovered phenotypes of *prt1* mutants.**

KEY WORDS

ubiquitination, proteolysis, E3 ligases, activity profiling, fluorescent dyes, labeling chemistry, protein labeling, N-end rule pathway

INTRODUCTION

The ON/OFF status of protein function within the cells' proteome, their general abundance and specific distribution throughout the compartments and therefore their functions and activities are precisely controlled by protein quality control (PQC) mechanisms to ensure proper life of any organism. Therefore, the biochemical analysis of the underlying mechanisms safeguarding proteostatic control is pivotal. It ranges from the molecular characterization of enzymes involved in PQC and their catalyzed reactions to enzyme-substrate and non-substrate protein-protein interactions. The so-called Ubiquitin (Ub) 26S proteasome system (UPS) is a master component of PQC with the key elements being non-catalytic Ub ligases (E3), the Ub-conjugating enzymes (E2), and the Ub-activating enzymes (E1).

To investigate an element conferring substrate specificity, we chose PROTEOLYSIS1 (PRT1) from *Arabidopsis thaliana* as a model E3 ligase, which is a *bona fide* single-subunit E3 with unknown substrate portfolio (Bachmair *et al.*, 1993; Potuschak *et al.*, 1998; Stary *et al.*, 2003). Its biological function remains elusive but it presumably represents a highly specific enzyme with E3 ligase function of the N-end rule pathway of targeted protein degradation, which is a part of the UPS. The N-end rule relates the half-life of a protein to its N-terminal amino acid (Bachmair *et al.*, 1986) and causes rapid proteolysis of proteins bearing so-called N-degrons, N-terminal sequences that lead to the degradation of the protein. N-degrons are created by endoproteolytic cleavage of protein precursors (pro-proteins) and represent the resulting neo-N-termini of the remaining C-terminal protein moiety, albeit not all freshly formed N-termini automatically present destabilizing residues (**Fig. 1a**).

The N-end rule pathway is an emerging vibrant area of research and has a multitude of functions in all kingdoms (Dougan *et al.*, 2010; Varshavsky, 2011; Tasaki *et al.*, 2012; Gibbs *et al.*, 2014a; Gibbs, 2015). Identified substrates are mainly important regulatory proteins and play key roles in animal and human health (Zenker *et al.*, 2005; Piatkov *et al.*, 2012; Brower *et al.*, 2013; Shemorry *et al.*, 2013; Kim *et al.*, 2014), plant stress response and agriculture (Gibbs *et al.*, 2011; Licausi *et al.*, 2011; Gibbs *et al.*, 2014a; Gibbs *et al.*, 2014b; Weits *et al.*, 2014; de Marchi *et al.*, 2016; Mendiondo *et al.*, 2016).

87 In plants, functions of N-end rule enzymes are associated with central developmen-
88 tal processes including seed ripening and lipid breakdown, hormonal signaling of abscisic
89 acid (ABA), gibberellin and ethylene, seed dormancy and germination (Holman *et al.*, 2009;
90 Abbas *et al.*, 2015; Gibbs *et al.*, 2015), leaf and shoot morphogenesis, flower induction, and
91 apical dominance (Graciet *et al.*, 2009), and the control of leaf senescence (Yoshida *et al.*,
92 2002). Then, the pathway was shown to be a sensor for molecular oxygen and reactive ox-
93 ygen species (ROS) by mediating nitric oxide (NO) signaling and regulating stress response
94 after hypoxia, e.g. after flooding and plant submergence (Gibbs *et al.*, 2011; Licausi *et al.*,
95 2011; Gibbs *et al.*, 2014b). A novel plant-specific class of enzymes was associated with the
96 pathway, i.e. plant cysteine oxidases (PCOs), highlighting plant-specific molecular circuits,
97 enzyme classes and mechanisms (Weits *et al.*, 2014). In the moss *Physcomitrella patens*, N-
98 end rule mutants are defective in gametophytic development (Schuessele *et al.*, 2016) and
99 protein targets of N-end rule-mediated posttranslational modifications were discovered
100 (Hoernstein *et al.*, 2016). Also in barley, the pathway is connected with development and
101 stress responses (Mendiondo *et al.*, 2016). Only very recently, a link between N-end rule
102 function and plant-pathogen response and innate immunity was found (de Marchi *et al.*,
103 2016), shedding light on novel functions of the yet underexplored branch of targeted pro-
104 teolysis. However, to date, the identity of plant N-end rule targets still remains obscure and
105 clear evidences from biochemical data of *in vitro* and *in vivo* studies such as N-terminal
106 sub-proteomics or enzymatic assays are still lacking.

107 A novel *in vivo* protein stabilization tool for genetic studies in developmental biology
108 and biotechnological applications, the 'lt-degron', works in plants and animals by directly
109 switching the levels of functional proteins *in vivo* (Faden *et al.*, 2016). The method is based
110 on conditional and specific PRT1-mediated protein degradation, the process studied in
111 depth with the here-generated fluorescent substrate reporters.

112 N-degrons are by definition recognized and the corresponding protein ubiquitinated
113 by specialized N-end rule E3 ligases, so-called *N-recognins* (Sriram *et al.*, 2011; Varshavsky,
114 2011; Tasaki *et al.*, 2012; Gibbs, 2015). In plants, only two of these, namely PRT1 and PRT6,
115 are associated with the N-end rule and assumed to function as N-recognins (**Fig. 1b**). This
116 is in contrast to the high number of proteolytically processed proteins which carry in their
117 mature form N-terminal amino acids that could potentially enter the enzymatic N-end rule

118 pathway cascade (Venne *et al.*, 2015). In the light of more than 800 putative proteases in
119 the model plant *Arabidopsis thaliana*, it is likely that the N-end rule pathway plays an im-
120 portant role for protein half-lives in a proteome-wide manner. Examples are found in the
121 METACASPASE9 degradome, i.e. that part of the proteome which is associated with degra-
122 dation (Tsiatsiani *et al.*, 2013), or the N-degradome of *E. coli* (Humbard *et al.*, 2013) with a
123 possibly analogous overlap with endosymbiotic plant organelles (Apel *et al.*, 2010).

124 PRT1, compared to the *Saccharomyces cerevisiae* N-recognin Ubr1 (225 kDa), is a
125 relatively small protein (46 kDa) and totally unrelated to any known eukaryotic N-
126 recognins but with functional similarities to prokaryotic homologs (**Fig. 1b**). It is therefore
127 perceived as a plant pioneer E3 ligase with both diversified mechanistics and function. Arti-
128 ficial substrate reporters based on mouse dihydrofolate reductase (DHFR) comprising an
129 N-terminal phenylalanine generated via the ubiquitin-fusion (UFT) technique lead to the
130 isolation of a *prt1* mutant in a forward mutagenesis screen (Bachmair *et al.*, 1993). In the
131 mutant cells and after MG132 treatment, the F-DHFR reporter construct was shown to be
132 stabilized whereas it was instable in the untreated wild type (Potuschak *et al.*, 1998; Stary
133 *et al.*, 2003). *PRT1* was able to heterologously complement a *Saccharomyces cerevisiae*
134 *ubr1Δ* mutant strain where Phe-, Tyr-, and Trp-initiated β-galactosidase test proteins were
135 stabilized. These reporters were rapidly degraded in *ubr1Δ* transformed with PRT1 (Stary
136 *et al.*, 2003). A new study revealed that cleavage of the E3 ligase BIG BROTHER by protease
137 DA1 forms a C-terminal, Tyr-initiated fragment. Its stability depends on the N-terminal
138 amino acid Tyr and the function of PRT1 E3 ligase (Dong *et al.*, 2016). However, until today,
139 there are no more *in vivo* targets or direct functions associated with PRT1, but recently, a
140 potential role of PRT1 in plant innate immunity was flagged (de Marchi *et al.*, 2016).

141 The spectrum of N-termini possibly recognized by plant N-end rule E3 ligases in-
142 cluding PRT1 is not sufficiently explored. Only Phe-starting test substrates were found to
143 be stabilized in a *prt1* mutant whereas initiation by Arg and Leu still caused degradation
144 (Potuschak *et al.*, 1998; Stary *et al.*, 2003; Garzón *et al.*, 2007). In the light of substrate iden-
145 tification, it is cardinal to determine PRT1 mechanistics in more detail because several
146 posttranslationally processed proteins bearing Phe, Trp and Tyr at the neo-N-termini were
147 found (Tsiatsiani *et al.*, 2013; Venne *et al.*, 2015) and hence represent putative PRT1 tar-

148 gets altogether. Elucidating the substrate specificity of PRT1 will be an important step for-
149 ward towards substrate identification and association of PRT1 and the N-end rule with a
150 biological context.

151 We established a technique that allows real time measurements of ubiquitination
152 using fluorescence scanning of SDS-PAGE gels and fluorescence polarization. We propose
153 its use as a generic tool for mechanistic and enzymological characterization of E3 ligases as
154 master components of the UPS directing substrate specificity. With a series of artificial test
155 substrates comprising various *bona fide* destabilizing N-end rule N-termini, substrate spec-
156 ificity was analyzed and revealed PRT1 preference for Phe as a representative of the bulky
157 hydrophobic class of amino acids. The methods commonly used to assay *in vitro* ubiquitina-
158 tion are based on end-time methods where the reaction is stopped at a given time point
159 and analyzed by SDS-PAGE followed by immunostaining with anti-Ub versus anti-target
160 specific antibodies. This detection via western blot often gives rise to the characteristic
161 hallmark of polyubiquitinated proteins, a "ubiquitination smear" or a more distinct "lad-
162 dering" of the posttranslationally Ub-modified target proteins. All the information of what
163 occurred during the time of reaction is unknown unless the assay is run at several different
164 time points which drastically increases both experimental time and reagent consumption.
165 Besides the most common methods used for ubiquitination assessment that involve immu-
166 nodetection with anti-Ub and anti-target antibodies, there are few other approaches mak-
167 ing use of different reagents. Comparable methods, their advantages and disadvantages are
168 listed in **Supporting Information Table S1**. The novelty offered by the present study is the
169 development of a fluorescence-based assay that allows real-time measurement of Ub in-
170 corporation in bulky solution eliminating shortcomings of the existing methods and thus a
171 more real mechanistic investigation. Our method monitors the ubiquitination process live,
172 in real time, using fluorescently labeled substrate proteins and fluorescence-based detec-
173 tion assays, namely fluorescence polarization (FP). In addition, the protocol was coupled to
174 fast and convenient scanning fluorescence in-gel detection. This type of assay can be easily
175 adapted for high-throughput measurements of ubiquitination activity and probably also
176 similar protein modification processes involving changes in substrate molecule properties
177 over time *in vitro*. Rather than merely analyzing enzyme–substrate or protein–protein in-
178 teractions, the here described method for the first time employs FP measurements for the

179 characterization of enzyme activity and parameters affecting the performance of the ubiq-
180 uitination reaction (Xia *et al.*, 2008; Kumar *et al.*, 2011; Smith *et al.*, 2013).
181 Here, we report a novel advanced approach to molecularly characterize E3 ligases,
182 to measure and track polyubiquitination live and in a time-resolved manner. It has the po-
183 tential to give rise to profound implications on our understanding of the interactions of E3
184 ligases with substrates and cofactors (non-substrates) and can impact ubiquitination re-
185 search in general as our work suggests to be transferable to other E3 ligases and enzyme-
186 substrate pairs. The method relies on rapid, easy and cheap protocols which are currently
187 lacking for in-depth biochemical analysis of E3 ligases and is at the same time non-
188 radioactive, sterically not interfering, and works with entire proteins in form of directly
189 labeled substrates.
190 So far, only three reports mention work on PRT1 at all, i.e. the two first brief descriptions
191 (Potuschak *et al.*, 1998; Stary *et al.*, 2003) and one highlighting the role of the N-end rule
192 pathway, in particular a novel function for PRT1, in plant immunity (de Marchi *et al.*, 2016).
193 However, the community lacks proofs demonstrating that PRT1 and other E3 candidates
194 are indeed involved in substrate protein ubiquitination. To date, ubiquitination activities
195 of E3 ligase candidates from the plant N-end rule pathway were only speculated.
196
197
198 **MATERIALS AND METHODS**

199 ***Cloning and expression of recombinant proteins***
200 *Artificial N-end rule substrates*
201 *Escherichia coli* flavodoxin (Flv, uniprot ID J7QH18) coding sequence was cloned directly
202 from *E. coli* DNA BL21(DE3) and flanked by an N-terminal triple hemagglutinin (HAT)
203 epitope sequence using the primers Flv_rvs (5‘-TTATTTGAGTAAATTAATCCACGATCC-3‘)
204 and Flv_eK_HAT(oh)_fwd (5‘-CTGGTGCTGCAGATATCACTCTTATCAGCGG-3‘). The X-eK se-
205 quences comprising codons for various N-terminal amino acids exposed after TEV cleavage
206 of the expressed X-eK-Flv fusion protein were cloned from an eK:HAT template using the
207 primers eK(X)_TEV(oh)_fwd (5’-GAGAATCTTTATTTTCAGxxx CACGGATCTGGAGCTTG-3’
208 with xxx=GTT (for Phe), GGG (for Gly), GAG (for Arg), and GTT (for Leu)) and

209 eK_HAT_flav(oh)_rvs (5'-CCGCTGATAAGAGTGATATCTGCAGCACCAG-3'). This sequence
210 contains a TEV protease recognition sequence (ENLYFQ|X with X being the neo-N-terminal
211 after cleavage, i.e. TEV P1' residue) at the N-terminal of the expressed X-eK-Flv fusion pro-
212 tein. In order to attach Gateway attB sites and fuse the PCR products, a PCR was performed
213 using Flv_attB2(oh)_rvs (5'-GGGACCACTTTGTACAAGAAAGCTGGGTA TCATTATTTGAG-
214 TAAATTAATCCACGATCC-3') and adapter_tev_fwd (5'-GGGGACAAGTTTG TACAAAAAA-
215 GCAGGCAGGCTTAGAAAACCTGTAT TTTCAGGGAATG-3'). All primer sequences are listed in
216 **Supporting Information Table S2**. An LR reaction into pVP16 (Thao *et al.*, 2004) (kind gift
217 from Russell L. Wrobel, University of Wisconsin-Madison) lead to the final construct that
218 consists of an N-terminal 8xHis:MBP double affinity tag. The expression vector
219 pVP16::8xHis:MBP:tev:eK:3xHA:Flv was transformed into *E. coli* BL21(DE3) and the fusion
220 protein was expressed by 0.2 mM IPTG induction in LB medium for 16 h at 26°C. Cells were
221 harvested via centrifugation (3,500 g, 4°C, 20 min), resuspended in Ni-buffer (50 mM sodi-
222 um phosphate pH 8.0, 300 mM NaCl), treated with 1mg/mL lysozyme (Sigma) in the pres-
223 ence of PMSF (Santa Cruz Biotechnology, sc-3597) added to a final concentration of 1 mM
224 followed by sonication (4 min 40 %, 6 min 60% intensity). The lysate was centrifuged
225 (12,500 g, 30 min), the supernatant loaded onto a Ni-NTA agarose column (Qiagen) equili-
226 brated with Ni-buffer, followed by Ni-buffer washing, then the protein was eluted with Ni-
227 buffer containing 200 mM imidaziole (Merck) and loaded onto amylose resin (NEB). After
228 washing with amylose-buffer (25 mM sodium phosphate pH 7.8, 150 mM NaCl), the protein
229 was eluted with amylose-buffer containing 10 mM maltose. For TEV digest, the fusion pro-
230 tein was incubated overnight at 4°C with 0.27 µg/µL self-made TEV protease, expressed
231 from pRK793 (Addgene, plasmid 8827), in 50 mM phosphate pH 8.0, 0.5 mM EDTA, 1 mM
232 DTT and loaded onto a Ni-agarose column (Qiagen) equilibrated with Ni-buffer. The flow-
233 through containing the tag-free X-eK-Flv substrate was concentrated with an Amicon Ultra-
234 15 (Merck Millipore).
235
236 *PRT1 cloning, expression and purification*
237 The coding sequence of *Arabidopsis* PRT1 was cloned according to gene annotations at
238 TAIR (www.arabidopsis.org) from cDNA. The Sequence was flanked by an N-terminal TEV
239 recognition sequence for facilitated downstream purification using the primers ss_prt1_tev

240 (5'-GCTTAGAGAATCTTTATTTTCAGGGGATGGCCGAAACTATGAAAGATATTAC-3') and
241 as_prt1_gw (5'-GGGTATCATTCTGTGCTTGATGACTCATTAG-3'). A second PCR using the
242 primers adapter (5'-GGGGACAAGTTTGTACAAAAAAGCAGGCTTAGAGAATCTTTATTTTCAG
243 GGG-3') and prt1_pos2_as (5'-GGGGACCACTTTGTACAAGAAAGCTGGGTATCATTCTGTGCTT
244 GATGA-3') was performed to amplify the construct to use it in a BP reaction for cloning into
245 pDONR201 (Invitrogen) followed by an LR reaction into the vector pVP16 (Thao *et al.*,
246 2004). Recombination into this Gateway destination vector containing a 8xHis:MBP coding
247 sequence 5' of the Gateway cassette leads to an N-terminal 8xHis:MBP double affinity tag.
248 The 8xHis:MBP:PRT1 isolation, cleavage and purification was done as described above for
249 the X-eK-Flv but the Ni-buffer contained 10% glycerol and 0.1% Tween 20.
250

251 ***Chemical labeling***

252 10 μM of purified X-eK-Flv was incubated for 1 h at room temperature with 100 μM of the
253 synthesized thiol reactive fluorogenic labeling dye in 20 mM Tris-Cl pH 8.3, 1 mM EDTA
254 and 1 mM tris(2-carboxy-ethyl)phosphine (TCEP, Thermo Scientific). The reaction was
255 stopped with 1 mM cysteine hydrochloride, the unreactive dye removed using 10 kDa cut-
256 off Amicon filters (Merck Millipore) by three successive washing steps, and the labeling
257 efficiency evaluated by fluorescence intensity of the labeled dye (Tecan M1000) and total
258 protein concentration using infra-red spectroscopy (Direct Detect, Merck Millipore).
259

260 ***Chemical synthesis***

261 The detailed synthesis protocols of the labeling probe NBD-NH-PEG_2-NH-haloacetamide
262 are described in **Supporting Information Methods**. In brief, the following synthesis steps
263 were accomplished: 1) tert-butyl {2-[2-(2-aminoethoxy)ethoxy)ethyl}carbamate (NH_2-
264 PEG_2-NHBoc); 2) NBD-NH-PEG_2-NHBoc; 3) NBD-NH-PEG_2-NH_2 hydrochloride; 4) NBD-NH-
265 PEG_2-NH-iodo-acetamide; 5) NBD-NH-PEG_2-NH-iodoacetamide; 6) NBD-NH-PEG_2-NH-
266 chloroacetamide.
267

268 ***tert*-butyl {2-[2-(2-aminoethoxy)ethoxy)ethyl}carbamate (NH_2-PEG_2-NHBoc)**

269 To a solution of 2,2'-(ethylenedioxy)-bis(ethylamine) (50.00 mL, 33.83 mmol; 495.6
270 %) in dry dioxane (190 mL), di-*tert*-butyl dicarbonate (14.90 g, 68.27 mmol, 100 %) in dry

dioxane (60 mL) was added slowly and the resulting mixture was stirred at 25 °C for 12 h. The reaction mixture was filtered, the solvent was removed under reduced pressure and the remaining residue was dissolved in distilled water (300 mL). The aqueous phase was extracted with dichloromethane (3 x 250 mL). Finally, the combined organic phases were dried (Na_2SO_4) and the solvent was removed under reduced pressure to yield *tert*-butyl {2-[2-(2-aminoethoxy)ethoxy)ethyl}carbamate (NH_2-PEG_2-NHBoc) as light yellow oil (16.09 g, 64.8 mmol, 94.9 %). ^{1}H NMR (400 MHz; $CDCl_3$) δ: 1.42 (br. s., 2H), 1.42 – 1.46 (m, 9H), 2.87 – 2.90 (m, 2H), 3.32 (m, 2H), 3.52 (m, , 2H), 3.55 (m, , 2H), 3.61 – 3.64 (m, 4H), 5.13 (br. s., 1H) ppm; ^{13}C NMR (100 MHz, $CDCl_3$) δ: 28.4, 40.3, 41.8, 67.1, 70.2, 73.5, 79.2, 156.0 ppm; ESI-MS m/z: 248.7 $[M + H]^+$, 497.4 $[2M + Na^+]^+$; HRMS (ESI) calculated for $C_{11}H_{25}N_2O_4$ 249.1809, found 249.1809.

NBD-NH-PEG$_2$-NHBoc

To a suspension of *tert*-butyl {2-[2-(2-aminoethoxy)ethoxy)ethyl}carbamate (1.50 g, 6.04 mmol, 100 %) and sodium bicarbonate (1.01 g, 12.08 mmol; 200 %) in acetonitrile (30 mL), 4-chloro-7-nitrobenzofurazan (NBD) (1.80 g, 9.06 mmol, 150 %) in acetonitrile (30 mL) was added slowly over a period of 2 h and the resulting mixture was stirred at 25 °C for 12 h. The reaction mixture was filtered, the solvent was removed under reduced pressure, and the remaining residue was subjected to chromatography (silica gel, methanol / ethyl acetate, 5 : 95) to yield NBD-NH-PEG$_2$-NHBoc as a brown solid (1.89 g, 4.58 mmol, 75.9 %). M.p.: 85 – 86 °C; R_F = 0.56 (methanol / ethyl acetate, 5 : 95); ^{1}H NMR (400 MHz; $CDCl_3$) δ [ppm]: 1.42 – 1.45 (m, 9H), 3.31 – 3.37 (m, 2H), 3.54 – 3.56 (m, 2H), 3.58 – 3.60 (m, 2H), 3.61 – 3.71 (m, 4 H), 3.87 (m, 2H), 5.02 (m, 1H), 6.20 (d, J = 8.6 Hz, 1H) , 6.88 (m, 1H), 8.49 (d, J = 8.6 Hz, 1H); ^{13}C NMR (100 MHz; $CDCl_3$) δ [ppm]: 28.4, 43.6, 68.1, 70.2, 70.2, 70.4, 70.5, 77.2, 98.7, 136.3, 143.9, 144.0, 144.0, 144.3, 155.9; ESI-MS m/z: 410.5 $[M - H]^+$, 434.2 $[M + Na]^+$, 845.4 $[2M + Na]^+$; HRMS (ESI) calculated for $C_{17}H_{25}N_5O_7Na$ 434.1646, found 434.1647.

NBD-NH-PEG$_2$-NH$_2$ hydrochloride

To a solution of NBD-NH-PEG$_2$-NHBoc (2.08 g, 5.06 mmol, 100 %) in dry methanol (20 mL), trimethylsilyl chloride (2.70 mL, 21.27 mmol, 500 %) was added *via* syringe and

the resulting mixture was stirred at 25 °C for 12 h. The solvent was removed under reduced pressure. The remaining residue was suspended in diethyl ether (15 mL), filtered and the solid was washed with several portions of diethyl ether, and the remaining solid was dried under reduced pressure to yield NBD-NH-PEG_2-NH_2 hydrochloride as a brown solid (1.56 g, 5.01 mmol, 98.9 %). The crude product was used without further purification. M.p.: 192 – 193 °C; ^{1}H NMR (400 MHz; CD_3OD) δ [ppm]: 3.09 – 3.11 (m, 2H), 3.64 – 3.76 (m, 8H), 3.87 – 3.90 (m, 2 H), 6.19 (d, *J* = 8.4 Hz, 1H), 8.45 (d, *J* = 8.7 Hz, 1H); ^{13}C NMR (100 MHz; CD_3OD) δ [ppm]: 41.5, 41.7, 70.1, 70.3, 70.8, 73.2, 98.8, 123.0, 136.5, 144.1, 144.4, 144.8; ESI-MS m/z: 310.5 $[M - 2H]^+$, 312.3 $[M]^+$; HRMS (ESI) calculated for $C_{12}H_{18}N_5O_5$ 312.1303, found 312.1303.

NBD-NH-PEG_2-NH-iodoacetamide

To a solution of NBD-NH-PEG_2-NH_2 hydrochloride (202.3 mg, 0.65 mmol; 100 %) and *N*,*N*'-diisopropylethylamine (134.3 µL, 0.77 mmol, 120 %) in dry acetonitril (4.0 mL), iodoacetic anhydride (401.0 mg, 1.13 mmol; 174 %) was added slowly and the resulting mixture was stirred at 25 °C for 12 h. The solvent was removed under reduced pressure and the remaining residue was subjected to chromatography (silica gel, methanol / ethyl acetate, 10 : 90) to yield NBD-NH-PEG_2-NH-iodoacetamide as a brown solid (151.1 mg, 0.32 mmol, 48.5 %). R_F = 0.45 (methanol / ethyl acetate, 10 : 90); ^{1}H NMR (400 MHz; $CDCl_3$) δ [ppm]: 3.50 – 3.54 (m, 2H), 3.62 – 3.65 (m, 2H), 3.69 – 3.71 (m, 8H), 3.73 – 3.76 (m, 2H), 6.21 (d, *J* = 8.7 Hz, 1H), 6.55 (br. s., 1H), 6.95 (br. s., 1H), 8.48 (d, J = 8.6 Hz, 1H); ^{13}C NMR (100 MHz; $CDCl_3$) δ [ppm]: 0.56, 40.1, 43.6, 68.1, 69.4, 70.3, 70.5, 136.4, 143.9, 144.3, 167.1; ESI-MS m/z: 478.3 $[M - H]^+$, 502.1 $[M + Na]^+$ + 981.3 $[2M + Na]^+$; HRMS (ESI (negative modus)) calculated for $C_{14}H_{17}N_5O_6I$ 478.0229, found 478.0222.

NBD-NH-PEG_2-NH-chloroacetamide

To a solution of NBD-NH-PEG_2-NH_2 hydrochloride (202.5 mg, 0.65 mmol; 100 %) and *N*,*N*'-diisopropylethylamine (134.3 µL, 0.77 mmol, 120 %) in dry acetonitril (4.0 mL), chloroacetic anhydride (221.7 mg, 1.30 mmol; 200 %) was added slowly and the resulting mixture was stirred at 25 °C for 12 h. The solvent was removed under reduced pressure and the remaining residue was subjected to chromatography (silica gel, methanol / ethyl

333 acetate, 10 : 90) to yield NBD-NH-PEG_2-NH-chloroacetamid as a brown solid (150.5 mg,
334 0.39 mmol, 59.7 %). R_F = 0.46 (methanol / ethyl acetate, 10 : 90); ^{1}H NMR (400 MHz; $CDCl_3$)
335 δ [ppm]: 3.54 – 3.58 (m, 2H), 3.64 – 3.75 (m, 8H), 3.87 – 3.90 (m, 2H), 4.06 (m, 2H), 6.20 (d,
336 *J* = 8.7 Hz, 1H), 6.90 (br. s., 1H), 6.98 (br. s., 1H), 8.48 (d, *J* = 8.6 Hz, 1H); ^{13}C NMR (100
337 MHz; $CDCl_3$) δ [ppm]: 30.51, 42.7, 43.6, 68.1, 69.5, 70.3, 70.5, 136.3, 143.9, 144.3, 166.0;
338 ESI-MS m/z: 386.1 $[M - H]^+$, 410.1 $[M + Na]^+$; HRMS (ESI (negative modus)) calculated for
339 $C_{14}H_{17}N_5O_6Cl$ 386.0873, found 386.0863.
340

341 ***Ubiquitination assay and in-gel fluorescence detection***

342 3.4 µM (total protein concentration, both label and unlabeled) of the X-eK-Flv fluorescently
343 labeled substrate (X-eK-Flv-NBD) were solved in 25 mM Tris-Cl pH 7.4, 50 mM KCl, 5 mM
344 $MgCl_2$, 0.7 mM DTT containing 16 µM Ub from bovine erythrocytes (Sigma-Aldrich, U6253).
345 For ubiquitination, 2 mM of ATP (New England Biolabs), 40 nM of E1[15], 0.31 µM of E2
346 (UBC8)[15], and 5 nM of E3 (8xHis:MBP-tagged or untagged PRT1) were added to the previ-
347 ous mix in a final volume of 30 µL and incubated at 30°C for 1 h. The reaction was stopped
348 by adding 5X reductive SDS-PAGE loading buffer and incubating for 10 min at 96 °C fol-
349 lowed by SDS-PAGE. The gels were scanned using fluorescence detection on a Typhoon FLA
350 9500 biomolecular imager (GE Healthcare) with a blue excitation laser (473 nm) LD and an
351 LBP emission filter (510LP), then blotted onto a cellulose membrane and detected with
352 either mouse monoclonal anti-Ub antibody (Ub (P4D1), sc-8017, Santa Cruz Biotechnology,
353 1:5,000 dilution in blocking solution [150 mM NaCl, 10 mM Tris-Cl pH 8, 3% skim milk
354 powder, 0.1% Tween 20]) or mouse monoclonal anti-HA epitope tag antibody (HA.11,
355 clone 16B12: MMS-101R, Covance; 1:1,000 to 1:5,000, in blocking solution) and goat anti-
356 mouse IgG-HRP (1858415, Pierce; 1:2,500 to 1:5,000 dilution in blocking solution). The
357 acquired images of the gels (prior blotting) were analyzed using the Gel Analyser densito-
358 metric soft (Gel.Analyser.com). Thus, one may use the same gel for both in-gel fluorescence
359 detection followed by blotting and immunodetection.
360 The same gels that were detected via fluorescence scanning were blotted and detected with
361 ECL without further processing such as stripping. Thus, fluorescent detection can be com-

362 bined with ECL in one simple workflow. For evaluation of pH dependence, 50 mM Tris-Cl
363 was used as a buffering agent at pH 6.75, 7.0, 7.5, 8.0, 8.5 and 9.0.
364
365 ***Real-time ubiquitination assay using fluorescence polarization***
366 For fluorescence polarization (FP), the reaction mixture (24 µL) containing all the compo-
367 nents except the ATP was incubated in a 384 well microplate (Corning, Cat. No. 3712 or
368 3764) at 30°C in a M1000 infinite plate reader (Tecan) until the temperature was stable
369 (typically 4-5 min) and the reaction triggered by adding 6 uL of 10 mM ATP preheated to
370 30°C. FP was monitored every 2 min at 562 nm while the excitation wavelength was set to
371 470 nm. The M1000 fluorescence polarization module was calibrated using 10 nM fluores-
372 cein in 10 mM NaOH at P = 20 mP.
373
374 ***Structure modeling of the artificial substrate***
375 The amino acid sequence of the artificial F-eK-Flv substrate was submitted to the Protein
376 Homology/Analogy Recognition Engine V 2.0 (Kelley *et al.*, 2015) (Phyre^2, Structural Bioin-
377 formatics Group, Imperial College, London) in both normal and intensive modes. The bests
378 selected templates were found to be PBD ID: 3EDC for the eK region and 2M6R for the Flv
379 part) and the model was visualized using ViewerLite (Accelrys Inc.).
380
381
382 **RESULTS**
383
384 **PRT1 is an E3 ubiquitin ligase and prefers bulky N-termini**
385 For the analysis of PRT1 E3 ligase function, i.e. recognition of N-end rule substrates,
386 we used recombinant PRT1 together with generic substrate reagents with unprecedented
387 detection features combining chemically synthesized fluorophores and recombinant ubiq-
388 uitination acceptors which were used as live protein modification detectors. To describe N-
389 terminal amino acid specificity of PRT1, the N-terminally variable protein parts of the re-
390 porters were engineered as N-terminal His8:MBP fusions comprising a recognition se-
391 quence of tobacco etch virus (TEV) protease at the junction to the subsequent generic sub-
392 strate protein moiety (**Fig. 2a, Supporting Information Fig.S 1a**). Cleavage by TEV gave

393 rise to small C-terminal fragments of the His8:MBP-substrate fusions of which the neo-N-
394 terminal, i.e. the P1' residue of the TEV cleavage site, can be altered to all proteinogenic
395 amino acids except proline (Kapust *et al.*, 2002; Phan *et al.*, 2002; Naumann *et al.*, 2016).
396 For a novel fluorescence-based approach, we covalently coupled a synthetic fluorescent
397 probe (**Fig. 2b**) to the artificial substrate protein. The resulting reagent served as fluores-
398 cent protein Ub acceptor in N-end rule ubiquitination assays. The architecture of the rea-
399 gent is as follows: after the cleavable His8:MBP tag, eK, a part of *E. coli* lacZ (Bachmair *et al.*,
400 1986) followed by a triple hemagglutinin epitope tag (3HA) for immunodetection and an *E.*
401 *coli* flavodoxin (Flv) were combined. Flv was chosen as a highly soluble and stable protein
402 and includes flavin mononucleotide as a cofactor. Its semiquinone is fluoresent but not sta-
403 ble enough to be used as fluorophore for detection in its plain form. Therefore, we decided
404 to additionally label the Flv protein. The junctions between His8:MBP and eK encode for
405 the N-termini glycin (Gly, G), phenylalanin (Phe, F), arginine (Arg, R), and leucin (Leu, L)
406 that get N-terminally exposed after TEV cleavage. The G/F/L/R-eK-Flv constructs contain a
407 single cysteine (Cys101 of Flv) that allowed the labeling of the purified recombinant fusion
408 protein with a novel thiol-reactive probe that comprises an iodoacetamide-polyethylene
409 glycol (PEG) linker and the fluorogenic subunit of 4-nitro-2,1,3-benzoxadiazole (NBD; **Fig.**
410 **2b**). We chose the latter due to its small size compared to other labeling reagents such as
411 large fluorescein moieties and because it can be detected very specifically by both UV ab-
412 sorption and UV fluorescence with low background interferences.

413 In an *in vitro* ubiquitination assay, we used recombinant UBC8 as a promiscuous E2
414 conjugating enzyme and UBA1 as E1 activating enzyme (Stegmann *et al.*, 2012) and show
415 here for the first time E3 ligase activity of PRT1 depending on E1, E2 and ATP (**Fig. 2c**).
416 PRT1 discriminated a substrate by its N-terminal, aiding the transfer of Ub to the substrate
417 and leading to polyubiquitination. After immunostaining with anti-Ub antibodies, usually, a
418 typical smear of higher molecular weight compared to the target protein's size is observed
419 or after probing with target-specific antibodies, a more or less distinct laddering, also of
420 high molecular weight, becomes evident. These are the common signs for polyubiquitina-
421 tion and a clear laddering was also visualized by fluorescent scanning in our novel ap-
422 proach. We identified distinct subspecies via in-gel detection (**Fig. 2c**). A classical end-time
423 point assay where the reaction was stopped at different reaction time points followed by

424 SDS-PAGE and in-gel fluorescence detection revealed the kinetics of PRT1 activity using F-
425 eK-Flv as substrate (**Fig. 2d**).
426 However, a real-time monitoring of the kinetic profile of the enzymatic reaction is
427 only possible via FP in live detection measurements. The kinetic profile is best-fitted with
428 an S-shaped curve and a growth curve model of logistic type (Richards' equation) rather
429 than exponentially as expected for simple kinetics (**Fig. 2e**).
430 It was previously suggested that PRT1 binds to N-degrons carrying bulky destabiliz-
431 ing residues (Stary *et al.*, 2003) but biochemical evidence for that was still lacking. By
432 changing the N-terminal residue of the X-eK-Flv-NBD substrate, it was possible to reveal
433 that PRT1 indeed discriminates the substrates according to the N-terminal residue, as ex-
434 pected (**Fig.2f, Supporting Information Fig. S1b,c**). While the substrates carrying G-, R-,
435 L-initiated N-termini showed poor ubiquitination, F-eK-Flv-NBD was heavily ubiquitinated.
436 While the eK-based substrate showed the kinetic curve discussed above, the control F-eΔK-
437 Flv substrate with mutated lysines (expected site of ubiquitination, Lys15 and Lys17, both
438 replaced by Arg) presented a faster initial rate of ubiquitination but levels of only half of
439 the final FP value (**Fig. 2f**). This is in good agreement with the in-gel fluorescence detection
440 where lower degrees of ubiquitination of F-eΔK-Flv, reduced mono- and di- ubiquitination -
441 but still clear polyubiquitination - were observed (**Supporting Information Fig. S1c**).
442 Another remarkable observation of the ubiquitination pattern in the in-gel fluores-
443 cence image (using three different independent substrate protein purifications of F-eK-Flv-
444 NBD) was that the tri-ubiquitinated form presents three distinct subspecies which eventu-
445 ally lead to a multitude of other species at higher level (**Supporting Information Fig. S1b**).
446 There was only one species of tri-ubiquitinated F-eΔK-Flv-NBD generated, where two
447 ubiquitination acceptors sites within eK (Lys15 and Lys17) were replaced by Arg (**Sup-**
448 **porting Information Fig. S1b**).
449

450 **Fluorescently labeled substrate proteins unravel mechanism of PRT1-mediated**
451 **ubiquitination**

452 The combination of the proposed two fluorescence-based methods allowed fast and
453 efficient *in vitro* investigation of the ubiquitination process via the E3 ligase PRT1 and the

454 optimization of the reaction conditions. As a first approach utilizing the real-time assay in
455 the context of substrate ubiquitination, we studied the role of changes in pH on the ubiqui-
456 tination process mediated by PRT1. A classical end-time approach revealed the reaction
457 optimum to be clearly above pH 7 but below pH 9 as indicated by the occurrence of
458 polyubiquitinated species of the fluorescent substrate probe F-eK-Flv-NBD (**Fig. 3a**). How-
459 ever, using our real-time FP protocol, we additionally acquired the kinetic profile of the
460 PRT1-mediated ubiquitination process (**Fig. 3b**) and the maximum reached polarization
461 values of this reaction (**Fig. 3c**). These correlated with the amount of polyubiqutinated spe-
462 cies detected in the SDS-PAGE gel-based end-time experiment (**Fig. 3a**) and the highest
463 initial rate (**Fig. 3c**) whereas the latter appears to be different from the reaction optimum
464 according to the detected max. FP. We also had previously observed, that F-eΔK-Flv ubiqui-
465 tination presented a faster initial rate but only half of the final FP (**Fig. 2f**) and lower de-
466 grees of final ubiquitination (**Supporting Information Fig. S1c**). Both bell-shaped forms of
467 the pH dependence for the highest initial reaction rate (pH 8.0) and the maximum sub-
468 strate polyubiquitination rate (pH 7.5) indicated two competing processes that generate a
469 local maximum (**Fig. 3c**).

470 A strong decrease of the ubiquitination rate mediated by PRT1 was observed at
471 higher concentrations of the E2-conjugating enzyme UBC8 (>2 μM) both via in-gel fluores-
472 cence (**Fig. 3d**) and FP (**Fig. 3e-g**). Based on the FP measurements using up to 2 μM of
473 UBC8, the K_M of substrate ubiquitination by PRT1 at different E2 concentrations was found
474 to be in the submicromolar range, 0.08±0.01 μM, indicating a very tight binding of the E2 to
475 PRT1 compared to other RING E3 ligases (Ye & Rape, 2009) (**Fig. 3e**). Moreover, the distri-
476 bution pattern of the ubiquitinated substrate species at the end of the reaction (**Fig. 3f**) and
477 the kinetic profiles of ubiquitination (**Fig. 3g**) are different, depending on the used E2 con-
478 centration.

479

480

481 **DISCUSSION**

482 The N-end rule pathway is an emerging vibrant area of research in plant sciences
483 and agriculture (Gibbs *et al.*, 2011; Licausi *et al.*, 2011; Gibbs *et al.*, 2014b; Weits *et al.*,
484 2014; de Marchi *et al.*, 2016; Mendiondo *et al.*, 2016) and reviewed in (Gibbs *et al.*, 2014a;

485 Gibbs, 2015; Gibbs *et al.*, 2016). Taking the first *bona fide* plant N-end rule E3 Ub ligase
486 PRT1 as the model, we describe a novel tool to molecularly characterize polyubiquitination
487 live, in real-time, and use it to gain the first mechanistic insights in PRT1 substrate prefer-
488 ence, activation and functional pairing with an E2-conjugating enzyme. To date, activity and
489 function of enzymatic N-end rule pathway components was only speculated and the field
490 was lacking investigations on molecular level. Here, we showed the first molecular evi-
491 dence for ubiquitination activity of an E3 ligase candidate from the entire plant N-end rule
492 pathway.

493 Here, we demonstrated PRT1 E3 Ub ligase activity and substrate preference by us-
494 ing recombinant PRT1 together with artificial protein substrates in an *in vitro* fluorescence-
495 based life ubiquitination assay. We found that first of all, the reporter construct based on
496 bacterial Flv chemically coupled to NBD (**Fig. 2b**) works as ubiquitination acceptor. Second,
497 this reaction reflects substrate specificity and cannot be considered an *in vitro* artifact,
498 since N-terminal amino acids other than Phe rendered the substrate a weaker target for
499 PRT1 (**Fig. 2f, Supporting Information Fig. S1b,c**). Third, our test system allowed to de-
500 scribe E3 ligase function and target specificity by using variants of labeled substrates.

501 Similar experiments are usually evaluated based on immunochemical and colori-
502 metric detection, incorporation of radioisotopes such as ^{125}I or ^{32}P, or fluorescently labeled
503 native or recombinant Ub (Ronchi & Haas, 2012; Melvin *et al.*, 2013; Lu *et al.*, 2015a; Lu *et*
504 *al.*, 2015b) (**Supporting Information Tab. S1**). However, problems of steric hindrance by
505 modifying Ub and difficulties to discriminate between auto- and substrate ubiquitination if
506 using labeled Ub may occur. Also artificial experimental setups such as single-molecule ap-
507 proaches or extreme buffer conditions might not represent or support formation of the
508 required complex ubiquitination machinery (**Supporting Information Table 1**). Our assay
509 allowed both direct assessment in the flow of the actual FP experiment and gel-based eval-
510 uation after completing SDS-PAGE. This renders protein transfer via western blotting plus
511 the subsequent time-consuming steps of blocking, immuno- and chemical detection obso-
512 lete. The protocol described is rapid, non-radioactive, uses only a small fluorophore as a
513 covalent dye, works with full substrate proteins instead of only peptides, and can be read
514 out live in real-time. Moreover, the FP approach conveys superimposable kinetic curves
515 with data from classical end-time point assays, but faster, with higher resolution in time

516 and using fewer reagents. The advantage of a combination of the described two fluores-
517 cence-based approaches, that is, gel-based and FP, is the possibility to gain mechanistic
518 insights which was not possible by applying only one of the single protocols. An example is
519 the determination of K_M and k_{cat} of the interaction of the E3 ligase PRT1 with E2-
520 conjugating enzymes. This included the influence of the E2 concentration on both the ubiq-
521 uitinated substrate species and the kinetic profile of the ubiquitination reaction.

522 Using FP coupled to immunoblot analysis, we were able to confirm that PRT1 is an
523 active E3 ligase acting in concert with E2-conjugating enzyme UBC8. In a buffer system
524 close to physiological conditions, it could be shown that PRT1 not only monoubiquitinates
525 N-degron containing substrates, but also mediates polyubiquitination without the aid of
526 further cofactors. Therefore, it was ruled out that PRT1 only monoubiquitinates which was
527 speculated previously (Stary *et al.*, 2003). Moreover, the action of a type II-N-recognin as
528 small as PRT1 (46 kDa) is most likely sufficient for subsequent target degradation by the
529 proteasome. Since PRT1 lacks the conserved ClpS domain that confers affinity to type II
530 substrates in other N-recognins, the binding mechanism of PRT1 to its substrate remains
531 an intriguing open question.

532 By FP-facilitated real-time monitoring of the kinetic profile of the PRT1-mediated
533 ubiquitination, we observed the S-shaped curve of the reaction (**Fig. 2e**). One explanation
534 for this kinetics and the presence of an initial lag phase is an increase of the affinity of PRT1
535 for the monoubiquitinated substrates compared to the non-ubiquitinated population. Pref-
536 erences of E2s and E3s for mono- or polyubiquitinated substrates and their influence on
537 ubiquitination velocity but also that initial ubiquitination greatly enhances the binding af-
538 finity of E3s to the substrate in subsequent reactions was shown previously (Sadowski &
539 Sarcevic, 2010; Lu *et al.*, 2015b). The chain elongation (Ub-Ub isopeptide bond formation)
540 can be faster than the chain initiation which might represent the rate limiting-step of the
541 reaction, rather than an E1-E2-controlled limiting-step. Thus, the chain elongation and
542 chain initiation steps appear to be distinct processes that have distinct molecular requisites
543 in agreement with previous findings for other E3s (Petroski & Deshaies, 2005; Deshaies &
544 Joazeiro, 2009). The lag phase is reduced if the rate is increased by higher concentration of
545 PRT1 (**Fig. 2e**).

546 The FP-based assay revealed that the kinetic profile of the ubiquitination was de-
547 pendent on the position and availability of lysines as Ub acceptor sites as suggested to be
548 characteristic of N-degrons (Bachmair & Varshavsky, 1989). By lowering the overall num-
549 ber of available lysines in the F-eΔK-Flv-NBD substrate (two Lys less than in X-eK-Flv con-
550 structs with 11 Lys in total) the overall ubiquitination was detectably reduced. Differences
551 in the kinetic curves of F-eK-Flv versus F-eΔK-Flv indicated that a reduction of the available
552 number of Lys residues lead to a faster initial rate of ubiquitination whereas the final FP
553 values reached only half of the levels compared to the assay applying the substrate with the
554 full set of Lys residues (**Fig. 2f**, **Supporting Information Fig. S1c**). However, the simple
555 gel-based end-point assay could not unravel if this was due to altered velocity of chain ini-
556 tiation versus chain elongation. The initiation per Lys residue was expected to be similar in
557 F-eK- versus F-eΔK-Flv substrates but chain elongation could apparently start faster in F-
558 eΔK-Flv. This demonstrated that the presence of E2 together with the particular substrate
559 plays a key role in the formation of the molecular assembly facilitating the ubiquitination
560 process. Already the intermolecular distance between the E3 ligase and the Ub acceptor
561 lysines of the substrate as well as the amino acid residues proximal to the acceptor lysines
562 determine the progress of the reaction and ubiquitination specificity (Sadowski & Sarcevic,
563 2010). Taking the slower initiation of polyubiquitination of F-eK-Flv into account, the avail-
564 ability of lysines at the N-terminus might interfere with the monoubiquitination of other,
565 more distal lysines and the E3 could remain associated with substrates that are monoubiq-
566 uitinated at the N-terminal.

567 When subjecting the F-eK-Flv-NBD substrate fusion protein to in vitro ubiquitina-
568 tion assays, three distinct subspecies of the tri-ubiquitinated form were detected versus
569 only one form, if F-eΔK-Flv-NBD was used (**Supporting Information Fig. S1c**). This could
570 be explained by a formation of various ubiquitinated isoforms of the substrate by utilizing
571 different lysine side chains as ubiquitination acceptor sites. These could be either within
572 the sequence of eK (e.g. Lys15 and Lys17) or within Flv (e.g. Lys100 and Lys222 which
573 seem structurally more favored according to the structural model, **Supporting Infor-**
574 **mation Fig. S1a**). This was further supported by the fact that there is only one species of
575 tri-ubiquitinated F-eΔK-Flv-NBD, where two ubiquitination acceptor sites within eK (Lys15
576 and Lys17) were replaced by Arg (**Supporting Information Fig. S1b**).

577 When analyzing the influence of the pH on PRT1 function as E3 Ub ligase, we docu-
578 mented bell-shaped forms of the pH dependence for the highest initial reaction rate (pH
579 8.0) and determined the maximum substrate polyubiquitination rate (pH 7.5). These indi-
580 cated two competing processes that generate a local maximum (**Fig. 3c**). In the light of re-
581 cently discussed mechanisms of E3 ligase action (Berndsen & Wolberger, 2014) and the
582 prediction of two RING domains in PRT1 (Stary *et al.*, 2003), higher ubiquitination rates
583 with increased pH could be due to deprotonation of the attacking lysine side chain of the E2
584 active site. This would facilitate thioester cleavage between E2 and Ub and thereby mediate
585 Ub transfer to the substrate lysines. A similar effect was observed regarding the influence
586 of the acidic residues in close vicinity of the E2 active site, which also cause deprotonation
587 of the lysine side chain of the incoming substrate (Plechanovova *et al.*, 2012). This possibly
588 explains the drastic increase in the initial rate of PRT1 substrate ubiquitination in the pH
589 6.8 to pH 8 range (**Fig. 3c**). The competing processes leading to the decrease in ubiquitina-
590 tion at pH>8 could be destabilization of ionic and hydrogen bonds at alkaline pH simply
591 interfering with protein-protein interaction or ATP hydrolysis affecting the Ub charging of
592 the E2 by the E1. This could also explain the premature leveling of the kinetic curves in the
593 FP measurements at pH>8 (**Fig. 3b**) while in a longer reaction timescale, the maximum FP
594 values would be expected to be the same from pH 6.8 to pH 7.5.

595 The apparent catalytic rate constant (k_{cat}) of the Ub transfer, more precisely the
596 transfer of the first Ub molecule, i.e. the rate limiting step, was found to be 1.30±0.07 s^{-1}.
597 This suggested that on the one hand PRT1 had a high turnover number due to a highly ac-
598 tive catalytic center and on the other hand that the E2 concentration does not only influ-
599 ence the rate of the Ub transfer to the substrate but also the mechanism itself. Possible
600 causes are the two separate and potentially distinctly favored chain initiation and elonga-
601 tion processes mentioned above. These could result in lowering the rate of the initiation
602 step at higher E2 concentrations since both the kinetic profile and the formation of ubiqui-
603 tinated species are affected and also the attacking lysines might be structurally differently
604 favored. This is especially suggested by the variable occurrence of the distinct pattern of
605 triubiquitinated substrate species (**Fig. 3d,f**) as mentioned above and discussed in other
606 systems as well (Ye & Rape, 2009).
607

608 By using fluorescently labeled substrate proteins in the two described approaches,
609 that is, gel-based fluorescence scanning after SDS-PAGE and FP, we were able to investigate
610 the mechanism of PRT1-mediated ubiquitination and optimize the reaction conditions. The
611 presented work serves as a model for the demonstration of differential mechanisms of sub-
612 strate recognition and tight interactor-binding in the N-end rule pathway.

613 PRT1 is a plant pioneer enzyme lacking homologs in the other kingdoms albeit small
614 and easy to produce in an active form as recombinant protein rendering it an exciting can-
615 didate for further functional and structural studies of key functions of one branch of the N-
616 end rule pathway. So far, only three research articles mention work on PRT1, i.e. the two
617 first brief descriptions (Potuschak *et al.*, 1998; Stary *et al.*, 2003) and one recently pub-
618 lished study highlighting the role of the N-end rule pathway - and in particular a novel func-
619 tion for PRT1 - in plant immunity (de Marchi *et al.*, 2016). However, to date, the community
620 lacks proofs demonstrating that PRT1 and other E3 candidates are indeed involved in sub-
621 strate protein ubiquitination.

622 The here described tool can be adopted by laboratories investigating N-end rule re-
623 lated posttranslational modifications such as deformylation, methionine excision, oxida-
624 tion, deamidation, arginylation, ubiquitination and degradation. Moreover, we are con-
625 vinced that it may also be extended to assays for other posttranslational modifications such
626 as phosphorylation and to other E3 Ub ligases as long as at least one native or artificial sub-
627 strate protein for the modification of interest is known. Because it makes use of chemical
628 labeling of substrate proteins rather than labeling protein modifiers such as Ub or phos-
629 phate themselves, one common reagent can be used for various modification assays. The
630 approach allows to measure and track posttranslational protein modification live and in a
631 time-resolved manner and has profound implications for our understanding of the interac-
632 tions of E3 ligases with substrates and non-substrates. Concerning the field of the N-end
633 rule pathway, this might apply to other candidates of E3 Ub ligases such as PROTEOLYSIS6
634 (PRT6) and BIG (AT3G02260) or potential N-end rule adapter proteins like PRT7
635 (AT4G23860) (Tasaki *et al.*, 2005; Garzón, 2008; Talloji, 2011). These experiments will be
636 of premier interest in the future because phenotypes of biological importance and genet-
637 ically determined causalities were described and need to be substantiated on molecular
638 level. Therefore, we see potential for a broader impact for ubiquitination research as it is

639 conceivable that the method is transferable to other E3 ligases and enzyme-substrate pairs.
640 In the course of our studies, we felt that rapid, easy and cheap protocols were lacking for
641 in-depth biochemical analysis of E3 ligase kinetics, the same holds true for non-radioactive
642 and sterically not interfering protocols and those where entire proteins and directly la-
643 beled substrates can be applied.

644 In terms of further applications, the kinetic approach allowed collecting data that
645 can assist to set up high-throughput assays, e.g. for screens of inhibitors and the influence
646 of small molecules potentially facilitating or enhancing ubiquitination. In our example, this
647 included testing of the enzymatic parameters of E2-E3 interactions and substrate specifici-
648 ties for PRT1. Similar approaches have used labeling with radionuclides or fluorescent dyes
649 coupled to Ub (Ronchi & Haas, 2012; Melvin *et al.*, 2013; Lu *et al.*, 2015a; Lu *et al.*, 2015b).
650 The latter covalent modification of Ub with fluorescent moieties is often impractical since
651 these groups can sterically hinder the E1-catalyzed activation and E2-dependent transthio-
652 lation reactions (Ronchi & Haas, 2012). This in turn can alter the rate-limiting step. The use
653 of radioactive isotopes requires at least running an SDS-PAGE and gel-drying or western
654 blotting followed by autoradiography for hours to days (**Supporting Information Tab. 1**).
655 Besides the described *in vitro* methods, several protocols and tools were successfully ap-
656 plied *in vivo*, mainly based on translational fusions of fluorescent proteins to degrons of the
657 Ub fusion degradation (UFD) pathway (Hamer *et al.*, 2010; Matilainen *et al.*, 2016), the N-
658 end rule pathway (Speese *et al.*, 2003; Faden *et al.*, 2016) or both (Dantuma *et al.*, 2000).
659 Other methods make use of Ub-binding systems to achieve various read-outs (Marblestone
660 *et al.*, 2012; Matilainen *et al.*, 2013)(**Supporting Information Tab. 1**).

661 In conclusion, we describe a system for real-time measurements of ubiquitination in
662 bulky solution with combined fluorescence scanning of SDS-PAGE gels and fluorescence
663 polarization. This setup was used to establish an artificial substrate protein-based detec-
664 tion reagent that reveals important mechanistic insights of E2-PRT1-substrate interaction.
665 We demonstrate for the first time that PRT1 is indeed involved in polyubiquitination of
666 substrate proteins depending on its N-terminal amino acid and therefore approached PRT1
667 as an player of the N-end rule pathway for the first time on a molecular level.
668
669

670 **ACKNOWLEDGEMENTS**

671 We thank Marco Trujillo for expression clones of His-tagged UBC8 and UBA1, discussions
672 and constant support in ubiquitination-related issues and Angela Schaks for synthesis of
673 the chemical probe. This work was supported by a grant for setting up the junior research
674 group of the *ScienceCampus Halle – Plant-based Bioeconomy* to N.D., by the grant WE
675 1467/13-1 of the German Research Foundation (Deutsche Forschungsgemeinschaft, DFG)
676 to B.W. funding E.P., a grant of the Leibniz-DAAD Research Fellowship Programme by the
677 Leibniz Association and the German Academic Exchange Service (DAAD) to A.C.M. and N.D.,
678 and Ph.D. fellowships of the Landesgraduiertenförderung Sachsen-Anhalt awarded to C.N.
679 and F.F. Financial support came from the Leibniz Association, the state of Saxony Anhalt,
680 the Deutsche Forschungsgemeinschaft (DFG) Graduate Training Center GRK1026 "*Confor-*
681 *mational Transitions in Macromolecular Interactions*" at Halle, and the Leibniz Institute of
682 Plant Biochemistry (IPB) at Halle, Germany. To complete work on this project, a Short Term
683 Scientific Mission (STSM) of the European Cooperation in Science and Technology (COST,
684 www.cost.eu) was granted to A.C.M. and N.D. by the COST Action BM1307 – "*European net-*
685 *work to integrate research on intracellular proteolysis pathways in health and disease (PRO-*
686 *TEOSTASIS)*". This work was partially funded by the grant DI 1794/3-1 of the German Re-
687 search Foundation to N.D.

688

689 **AUTHOR CONTRIBUTION**

690 A.C.M. performed the ubiquitination reactions and related analysis. E.P. and B.W. designed
691 and synthesized the fluorescent probe, B.W. supervised the chemical synthesis, M.K. estab-
692 lished PRT1 ubiquitination reactions, C.N. cloned and purified PRT1, F.F. cloned the X-eK-
693 HAT fragment and performed site-directed mutagenesis. N.D. and A.C.M. designed the
694 study, wrote the manuscript under consultation with all co-authors and designed the fig-
695 ures. All authors read and approved the final version of this manuscript.

696 ## REFERENCES

697 **Abbas M, Berckhan S, Rooney DJ, Gibbs DJ, Vicente Conde J, Sousa Correia C, Bassel GW, Marin-de la**
698 **Rosa N, Leon J, Alabadi D, et al. 2015.** Oxygen sensing coordinates photomorphogenesis to
699 facilitate seedling survival. *Curr Biol* **25**(11): 1483-1488.
700 **Apel W, Schulze W, Bock R. 2010.** Identification of protein stability determinants in chloroplasts. *Plant J*
701 **63**(4): 636-650.
702 **Bachmair A, Becker F, Schell J. 1993.** Use of a reporter transgene to generate arabidopsis mutants in
703 ubiquitin-dependent protein degradation. *Proc Natl Acad Sci U S A* **90**(2): 418-421.
704 **Bachmair A, Finley D, Varshavsky A. 1986.** In vivo half-life of a protein is a function of its amino-terminal
705 residue. *Science* **234**(4773): 179-186.
706 **Bachmair A, Varshavsky A. 1989.** The degradation signal in a short-lived protein. *Cell* **56**(6): 1019-1032.
707 **Berndsen CE, Wolberger C. 2014.** New insights into ubiquitin E3 ligase mechanism. *Nat Struct Mol Biol*
708 **21**(4): 301-307.
709 **Brower CS, Piatkov KI, Varshavsky A. 2013.** Neurodegeneration-associated protein fragments as short-
710 lived substrates of the N-end rule pathway. *Mol Cell* **50**(2): 161-171.
711 **Dantuma N, Lindsten K, Glas R, Jellne M, Masucci M. 2000.** Short-lived green fluorescent proteins for
712 quantifying ubiquitin/proteasome-dependent proteolysis in living cells. *Nat Biotechnol* **18**(5):
713 538-543.
714 **de Marchi R, Sorel M, Mooney B, Fudal I, Goslin K, Kwasniewska K, Ryan PT, Pfalz M, Kroymann J,**
715 **Pollmann S, et al. 2016.** The N-end rule pathway regulates pathogen responses in plants. *Sci Rep*
716 **6**: 26020.
717 **Deshaies RJ, Joazeiro CA. 2009.** RING domain E3 ubiquitin ligases. *Annu Rev Biochem* **78**: 399-434.
718 **Dong H, Dumenil J, Lu F, Na L, Vanhaeren H, Naumann C, Klecker M, Prior R, Smith C, McKenzie N, et**
719 **al. 2016.** A novel ubiquitin-activated peptidase regulates organ size in Arabidopsis by cleaving
720 growth regulators that promote cell proliferation and inhibit endoreduplication. *bioRxiv*.
721 **Dougan D, Truscott K, Zeth K. 2010.** The bacterial N-end rule pathway: expect the unexpected. *Mol*
722 *Microbiol* **76**(3): 545-558.
723 **Faden F, Ramezani T, Mielke S, Almudi I, Nairz K, Froehlich MS, Hockendorff J, Brandt W,**
724 **Hoehenwarter W, Dohmen RJ, et al. 2016.** Phenotypes on demand via switchable target protein
725 degradation in multicellular organisms. *Nat Commun* **7**: 12202.
726 **Garzón M. 2008.** *Links between the Ubiquitin-Proteasome System and Cell Death Pathways in*
727 *Arabidopsis thaliana.* Dissertation Cologne.
728 **Garzón M, Eifler K, Faust A, Scheel H, Hofmann K, Koncz C, Yephremov A, Bachmair A. 2007.**
729 PRT6/At5g02310 encodes an Arabidopsis ubiquitin ligase of the N-end rule pathway with
730 arginine specificity and is not the CER3 locus. *FEBS Lett* **581**(17): 3189-3196.
731 **Gibbs DJ. 2015.** Emerging Functions for N-Terminal Protein Acetylation in Plants. *Trends Plant Sci* **20**(10):
732 599-601.
733 **Gibbs DJ, Bacardit J, Bachmair A, Holdsworth MJ. 2014a.** The eukaryotic N-end rule pathway: conserved
734 mechanisms and diverse functions. *Trends Cell Biol* **24**(10): 603-611.
735 **Gibbs DJ, Bailey M, Tedds HM, Holdsworth MJ. 2016.** From start to finish: amino-terminal protein
736 modifications as degradation signals in plants. *New Phytol*.
737 **Gibbs DJ, Conde JV, Berckhan S, Prasad G, Mendiondo GM, Holdsworth MJ. 2015.** Group VII Ethylene
738 Response Factors Coordinate Oxygen and Nitric Oxide Signal Transduction and Stress Responses
739 in Plants. *Plant Physiol* **169**(1): 23-31.
740 **Gibbs DJ, Lee SC, Isa NM, Gramuglia S, Fukao T, Bassel GW, Correia CS, Corbineau F, Theodoulou FL,**
741 **Bailey-Serres J, et al. 2011.** Homeostatic response to hypoxia is regulated by the N-end rule
742 pathway in plants. *Nature* **479**(7373): 415-418.

743 **Gibbs DJ, Md Isa N, Movahedi M, Lozano-Juste J, Mendiondo GM, Berckhan S, Marin-de la Rosa N,**
744 **Vicente Conde J, Sousa Correia C, Pearce SP, et al. 2014b.** Nitric oxide sensing in plants is
745 mediated by proteolytic control of group VII ERF transcription factors. *Mol Cell* **53**(3): 369-379.
746 **Graciet E, Walter F, Ó'Maoiléidigh D, Pollmann S, Meyerowitz E, Varshavsky A, Wellmer F. 2009.** The
747 N-end rule pathway controls multiple functions during Arabidopsis shoot and leaf development.
748 *Proc Natl Acad Sci U S A* **106**(32): 13618-13623.
749 **Hamer G, Matilainen O, Holmberg CI. 2010.** A photoconvertible reporter of the ubiquitin-proteasome
750 system in vivo. *Nat Methods* **7**(6): 473-478.
751 **Hoernstein SN, Mueller SJ, Fiedler K, Schuelke M, Vanselow JT, Schuessele C, Lang D, Nitschke R, Igloi**
752 **GL, Schlosser A, et al. 2016.** Identification of targets and interaction partners of arginyl-tRNA
753 protein transferase in the moss Physcomitrella patens. *Mol Cell Proteomics*.
754 **Holman T, Jones P, Russell L, Medhurst A, Ubeda Tomas S, Talloji P, Marquez J, Schmuths H, Tung S,**
755 **Taylor I, et al. 2009.** The N-end rule pathway promotes seed germination and establishment
756 through removal of ABA sensitivity in Arabidopsis. *Proc Natl Acad Sci U S A* **106**(11): 4549-4554.
757 **Humbard M, Surkov S, De Donatis G, Jenkins L, Maurizi M. 2013.** The N-degradome of escherichia coli:
758 limited proteolysis in vivo generates a large pool of proteins bearing N-degrons. *J Biol Chem*
759 **288**(40): 28913-28924.
760 **Kapust R, Tozser J, Copeland T, Waugh D. 2002.** The P1' specificity of tobacco etch virus protease.
761 *Biochem Biophys Res Commun* **294**(5): 949-955.
762 **Kelley LA, Mezulis S, Yates CM, Wass MN, Sternberg MJ. 2015.** The Phyre2 web portal for protein
763 modeling, prediction and analysis. *Nat Protoc* **10**(6): 845-858.
764 **Kim H, Kim R, Oh J, Cho H, Varshavsky A, Hwang C. 2014.** The N-Terminal Methionine of Cellular
765 Proteins as a Degradation Signal. *Cell* **156**(1-2): 158-169.
766 **Kumar E, Charvet C, Lokesh G, Natarajan A. 2011.** High-throughput fluorescence polarization assay to
767 identify inhibitors of Cbl(TKB)-protein tyrosine kinase interactions. *Anal Biochem* **411**(2): 254-
768 260.
769 **Licausi F, Kosmacz M, Weits DA, Giuntoli B, Giorgi FM, Voesenek LA, Perata P, van Dongen JT. 2011.**
770 Oxygen sensing in plants is mediated by an N-end rule pathway for protein destabilization.
771 *Nature* **479**(7373): 419-422.
772 **Lu Y, Lee BH, King RW, Finley D, Kirschner MW. 2015a.** Substrate degradation by the proteasome: a
773 single-molecule kinetic analysis. *Science* **348**(6231): 1250834.
774 **Lu Y, Wang W, Kirschner MW. 2015b.** Specificity of the anaphase-promoting complex: a single-molecule
775 study. *Science* **348**(6231): 1248737.
776 **Marblestone JG, Larocque JP, Mattern MR, Leach CA. 2012.** Analysis of ubiquitin E3 ligase activity using
777 selective polyubiquitin binding proteins. *Biochim Biophys Acta* **1823**(11): 2094-2097.
778 **Matilainen O, Arpalahti L, Rantanen V, Hautaniemi S, Holmberg CI. 2013.** Insulin/IGF-1 signaling
779 regulates proteasome activity through the deubiquitinating enzyme UBH-4. *Cell Rep* **3**(6): 1980-
780 1995.
781 **Matilainen O, Jha S, Holmberg CI. 2016.** Fluorescent Tools for In Vivo Studies on the Ubiquitin-
782 Proteasome System. *Methods Mol Biol* **1449**: 215-222.
783 **Melvin A, Woss G, Park J, Dumberger L, Waters M, Allbritton N. 2013.** A comparative analysis of the
784 ubiquitination kinetics of multiple degrons to identify an ideal targeting sequence for a
785 proteasome reporter. *PLoS One* **8**(10): e78082.
786 **Mendiondo GM, Gibbs DJ, Szurman-Zubrzycka M, Korn A, Marquez J, Szarejko I, Maluszynski M, King J,**
787 **Axcell B, Smart K, et al. 2016.** Enhanced waterlogging tolerance in barley by manipulation of
788 expression of the N-end rule pathway E3 ligase PROTEOLYSIS6. *Plant Biotechnol J* **14**(1): 40-50.
789 **Naumann C, Mot AC, Dissmeyer N. 2016.** Generation of Artificial N-end Rule Substrate Proteins In Vivo
790 and In Vitro. *Methods Mol Biol* **1450**: 55-83.

791 **Petroski MD, Deshaies RJ. 2005.** Mechanism of lysine 48-linked ubiquitin-chain synthesis by the cullin-
792 RING ubiquitin-ligase complex SCF-Cdc34. *Cell* **123**(6): 1107-1120.
793 **Phan J, Zdanov A, Evdokimov A, Tropea J, Peters H, Kapust R, Li M, Wlodawer A, Waugh D. 2002.**
794 Structural basis for the substrate specificity of tobacco etch virus protease. *J Biol Chem* **277**(52):
795 50564-50572.
796 **Piatkov K, Brower C, Varshavsky A. 2012.** The N-end rule pathway counteracts cell death by destroying
797 proapoptotic protein fragments. *Proc Natl Acad Sci U S A* **109**(27): E1839-1847.
798 **Plechanovova A, Jaffray EG, Tatham MH, Naismith JH, Hay RT. 2012.** Structure of a RING E3 ligase and
799 ubiquitin-loaded E2 primed for catalysis. *Nature* **489**(7414): 115-120.
800 **Potuschak T, Stary S, Schlogelhofer P, Becker F, Nejinskaia V, Bachmair A. 1998.** PRT1 of Arabidopsis
801 thaliana encodes a component of the plant N-end rule pathway. *Proc Natl Acad Sci U S A* **95**(14):
802 7904-7908.
803 **Ronchi VP, Haas AL. 2012.** Measuring rates of ubiquitin chain formation as a functional readout of ligase
804 activity. *Methods Mol Biol* **832**: 197-218.
805 **Sadowski M, Sarcevic B. 2010.** Mechanisms of mono- and poly-ubiquitination: Ubiquitination specificity
806 depends on compatibility between the E2 catalytic core and amino acid residues proximal to the
807 lysine. *Cell Div* **5**: 19.
808 **Schuessele C, Hoernstein SN, Mueller SJ, Rodriguez-Franco M, Lorenz T, Lang D, Igloi GL, Reski R. 2016.**
809 Spatio-temporal patterning of arginyl-tRNA protein transferase (ATE) contributes to
810 gametophytic development in a moss. *New Phytol* **209**(3): 1014-1027.
811 **Shemorry A, Hwang C, Varshavsky A. 2013.** Control of protein quality and stoichiometries by N-terminal
812 acetylation and the N-end rule pathway. *Mol Cell* **50**(4): 540-551.
813 **Smith M, Scaglione K, Assimon V, Patury S, Thompson A, Dickey C, Southworth D, Paulson H,**
814 **Gestwicki J, Zuiderweg E. 2013.** The E3 ubiquitin ligase CHIP and the molecular chaperone
815 Hsc70 form a dynamic, tethered complex. *Biochemistry* **52**(32): 5354-5364.
816 **Speese S, Trotta N, Rodesch C, Aravamudan B, Broadie K. 2003.** The ubiquitin proteasome system
817 acutely regulates presynaptic protein turnover and synaptic efficacy. *Curr Biol* **13**(11): 899-910.
818 **Sriram S, Kim B, Kwon Y. 2011.** The N-end rule pathway: emerging functions and molecular principles of
819 substrate recognition. *Nat Rev Mol Cell Biol* **12**(11): 735-747.
820 **Stary S, Yin X, Potuschak T, Schlogelhofer P, Nizhynska V, Bachmair A. 2003.** PRT1 of Arabidopsis is a
821 ubiquitin protein ligase of the plant N-end rule pathway with specificity for aromatic amino-
822 terminal residues. *Plant Physiol* **133**(3): 1360-1366.
823 **Stegmann M, Anderson RG, Ichimura K, Pecenkova T, Reuter P, Zarsky V, McDowell JM, Shirasu K,**
824 **Trujillo M. 2012.** The ubiquitin ligase PUB22 targets a subunit of the exocyst complex required
825 for PAMP-triggered responses in Arabidopsis. *Plant Cell* **24**(11): 4703-4716.
826 **Talloji P. 2011.** *Identification of novel components and links in ubiquitin dependent protein degradation*
827 *pathways of Arabidopsis thaliana.* Dissertation, University of Cologne Cologne.
828 **Tasaki T, Mulder L, Iwamatsu A, Lee M, Davydov I, Varshavsky A, Muesing M, Kwon Y. 2005.** A family
829 of mammalian E3 ubiquitin ligases that contain the UBR box motif and recognize N-degrons. *Mol*
830 *Cell Biol* **25**(16): 7120-7136.
831 **Tasaki T, Sriram S, Park K, Kwon Y. 2012.** The N-end rule pathway. *Annu Rev Biochem* **81**: 261-289.
832 **Thao S, Zhao Q, Kimball T, Steffen E, Blommel P, Riters M, Newman C, Fox B, Wrobel R. 2004.** Results
833 from high-throughput DNA cloning of Arabidopsis thaliana target genes using site-specific
834 recombination. *J Struct Funct Genomics* **5**(4): 267-276.
835 **Tsiatsiani L, Timmerman E, De Bock PJ, Vercammen D, Stael S, van de Cotte B, Staes A, Goethals M,**
836 **Beunens T, Van Damme P, et al. 2013.** The Arabidopsis metacaspase9 degradome. *Plant Cell*
837 **25**(8): 2831-2847.

838 **Varshavsky A. 2011.** The N-end rule pathway and regulation by proteolysis. *Protein Sci* **20**(8): 1298-
839 1345.
840 **Venne AS, Solari FA, Faden F, Paretti T, Dissmeyer N, Zahedi RP. 2015.** An improved workflow for
841 quantitative N-terminal charge-based fractional diagonal chromatography (ChaFRADIC) to study
842 proteolytic events in Arabidopsis thaliana. *Proteomics* **15**(14): 2458-2469.
843 **Weits D, Giuntoli B, Kosmacz M, Parlanti S, Hubberten H, Riegler H, Hoefgen R, Perata P, van Dongen J,**
844 **Licausi F. 2014.** Plant cysteine oxidases control the oxygen-dependent branch of the N-end-rule
845 pathway. *Nat Commun* **5**: 3425.
846 **Xia Z, Webster A, Du F, Piatkov K, Ghislain M, Varshavsky A. 2008.** Substrate-binding sites of UBR1, the
847 ubiquitin ligase of the N-end rule pathway. *J Biol Chem* **283**(35): 24011-24028.
848 **Ye Y, Rape M. 2009.** Building ubiquitin chains: E2 enzymes at work. *Nat Rev Mol Cell Biol* **10**(11): 755-
849 764.
850 **Yoshida S, Ito M, Callis J, Nishida I, Watanabe A. 2002.** A delayed leaf senescence mutant is defective in
851 arginyl-tRNA:protein arginyltransferase, a component of the N-end rule pathway in Arabidopsis.
852 *Plant J* **32**(1): 129-137.
853 **Zenker M, Mayerle J, Lerch M, Tagariello A, Zerres K, Durie P, Beier M, Hulskamp G, Guzman C, Rehder**
854 **H, et al. 2005.** Deficiency of UBR1, a ubiquitin ligase of the N-end rule pathway, causes
855 pancreatic dysfunction, malformations and mental retardation (Johanson-Blizzard syndrome).
856 *Nat Genet* **37**(12): 1345-1350.
857

858

FIGURES

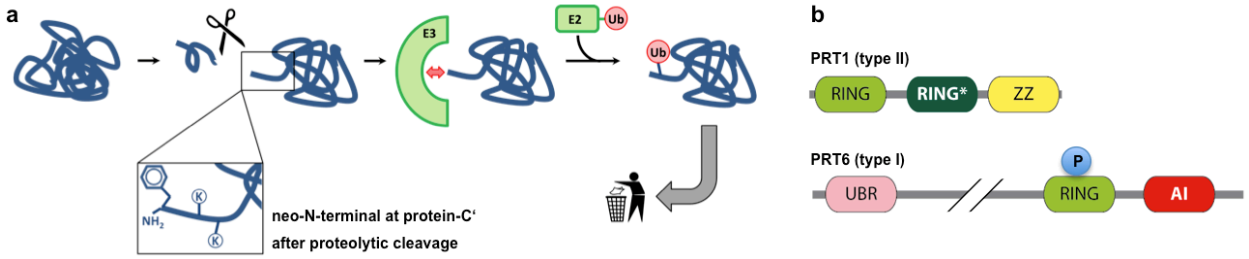

Figure 1. Generation of N-end rule substrates by proteolytic processing and predicted features of the two *bona fide* plant N-recognins. a) Substrates containing N-degrons can be generated from (pre-)pro-proteins as precursor sequences after proteolytic cleavage (indicated by the scissors). The N-degron shown here comprises a Phe residue as primary destabilizing residue at the protein-C' and internal lysines for polyubiquitination. These N-degrons can be recognized by N-end rule E3 Ub ligases (N-recognins) which in turn associate with Ub-conjugating enzymes (E2) carrying Ub which was previously activated by E1 enzymes. One possible result of ubiquitination is protein degradation and to date, in the context of the N-end rule, ubiquitination is assumed to lead to degradation in most of the cases. **b)** The two known *Arabidopsis* N-recognins were identified by their function (PRT1, 46 kDa) and by homology to the UBR-box from *S. cerevisiae* UBR1p (PRT6, 224 kDa). UBR: box binding type I substrates; RING*: composite domain containing RING and CCCH-type Zn fingers; ZZ: Zinc binding domain similar to RING; RING: protein-protein interaction domain for E2–E3 interaction; AI: predicted autoinhibitory domain (intramolecular interaction); P: phosphorylation site (PhosPhAt 4.0; phosphat.uni-hohenheim.de). b is modified from Tasaki et al., 2012.

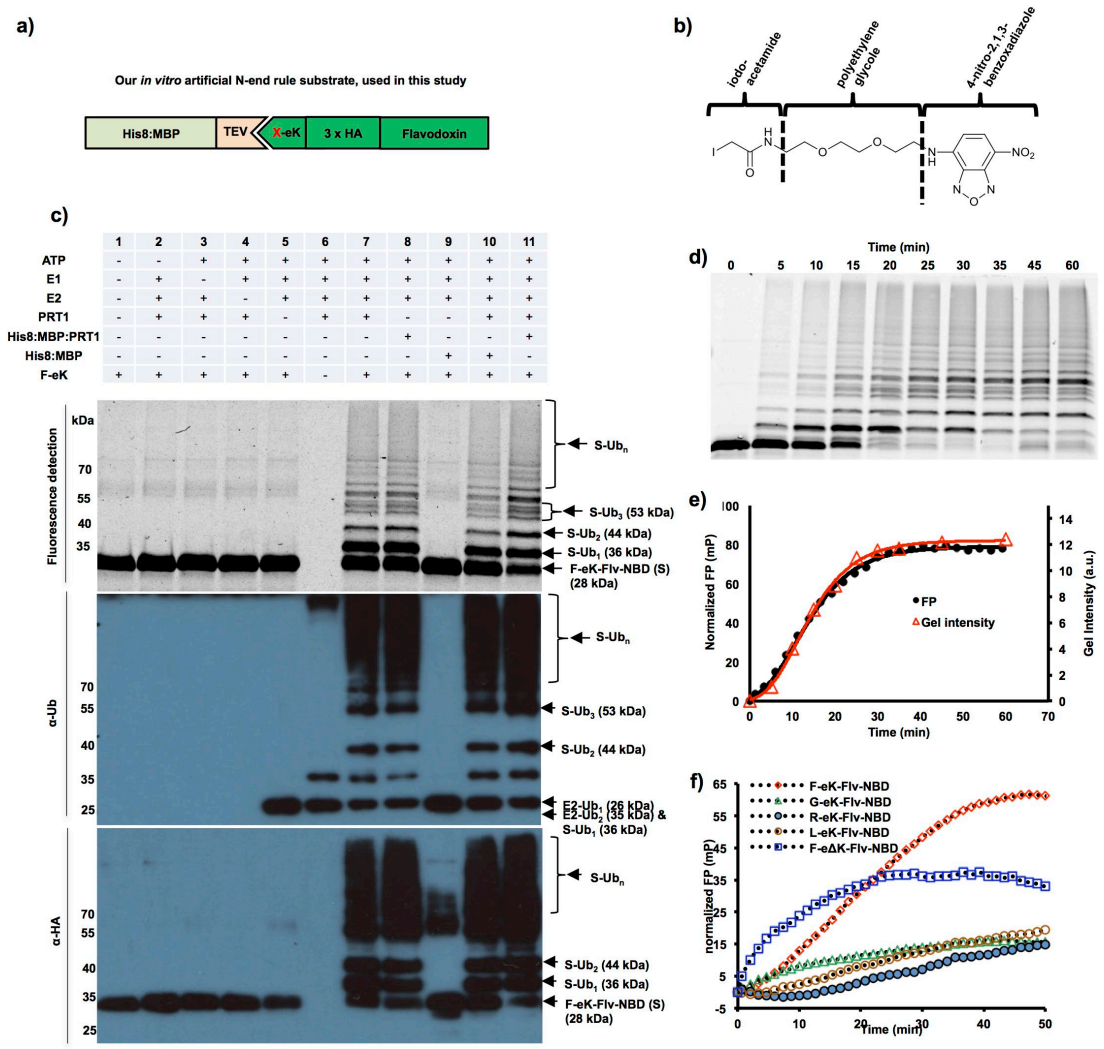

Figure 2. Fluorescent protein conjugates for monitoring *in vitro* substrate ubiquitination in real time. a) Design of recombinant fusion proteins used as N-end rule substrates. After TEV cleavage and removal of the His8:MBP affinity tag, the artificial substrate based on *E. coli* flavodoxin (Flv) is initiated with a neo-N-terminal, here Phe (F), Gly (G), Leu (L) or Arg (R). **b)** Skeletal formula of the synthesized thiol-reactive fluorescent compound. The substrate was covalently tagged with the reagent composed of iodoacetamide, polyethylene glycol (PEG) linker and 4-nitro-2,1,3-benzoxadiazole (NBD). The reactive iodine-containing group on the left couples to the thiol group of internal Cys residues of Flv. NBD serves as a fluorophore with excitation at 470 nm and emission at 520 nm. **c)** Detection via fluorescence and immunoblotting of the F-eK-Flv-NBD after *in vitro* ubiquitination. The labeled protein and its ubiquitinated variants were detected via fluorescence scanning directly from the SDS-PAGE gel followed by western blotting and immunodetection with anti-HA and anti-Ub antibodies. Lane 6 shows ubiquitinated E2 like in all lanes and autoubiquitination of PRT1 as very high molecular weight 'smear'. Cleaved PRT1 as well as His8:MBP-tagged PRT1 were used together with His:UBA1 (E1) and His:UBC8 (E2) (Stegmann *et al.*, 2012). **d and e)** Kinetic profiles of PRT1-mediated ubiquitination. F-eK-Flv-NBD ubiquitination was monitored by FP and in-gel fluorescence scanning. The S-shaped kinetic curve is observed in both in-gel fluorescence scanning detection and fluorescence polarization. **f)** N-terminal specificity evaluated by real-time ubiquitination detec-

892 tion. Fluorescently labelled R-eK-Flv, L-eK-Flv, G-eK-Flv, F-eΔK-Flv and F-eK-Flv were comparatively evaluated for their
893 degree of ubiquitination by PRT1.

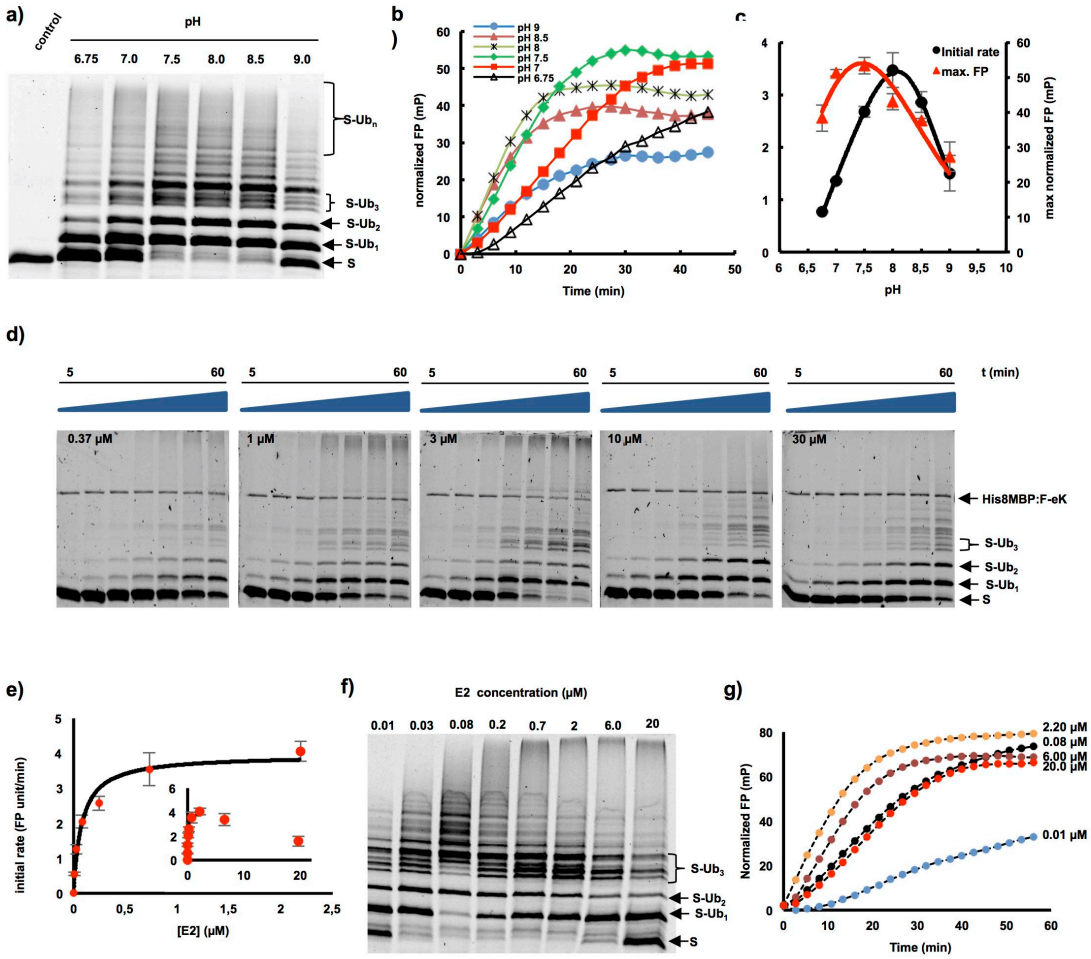

Figure 3. Applications of fluorescent protein conjugates for monitoring pH dependent ubiquitination and enzymatic parameters of PRT1 E3 ligase. a-c) pH dependent ubiquitination of the F-eK-Flv substrate. **a)** In-gel detection of F-eK-Flv ubiquitinated species after 1 h reaction at several pH values demonstrating different patterns of polyubiquitination preferences depending on the pH. **b)** Kinetic profiles, **c)** initial rates and maximum end-time FP values forming a bell-shaped distribution depending on the pH. **d-g)** PRT1-mediated ubiquitination of F-ek-Flv dependent on the concentration of E2-conjugating enzyme (UBC8). **d)** Time dependence of ubiquitination at several E2 concentrations for the first 60 min at 5 nM PRT1, time scale: 5-60 min. **e)** Michaelis-Menten curve plotted using the initial rate from FP data suggest an E2-driven inhibition effect. **f)** The qualitative evaluation of ubiquitination was done using in-gel scanning fluorescence and **g)** kinetic profiles were obtained using FP measurements, similar conditions as in d) but with ten times higher concentration of PRT1, i.e. 50 nM.

907 **SUPPORTING INFORMATION**

908

909 Additional supporting information may be found in the online version of this article.

910

911 **SUPPORTING FIGURES**

912 **Supporting Information Figure 1. Modeled structure of the F-eK-Flv substrate and**
913 **PRT1 N-terminal specificity.**

914

915 **SUPPORTING TABLES**

916 **Supporting Information Table 1. State-of-the-art ubiquitination detection methods.**

917 **Supporting Information Table 2. Oligonucleotides used in this study.**

918

919 **SUPPORTING METHODS**

920 **Synthesis of the chemical probe NBD-NH-PEG$_2$-NH-haloacetamide.**

921

922 **SUPPORTING REFERENCES**